33rd EPS Conference on Plasma Phys. Rome, 19 - 23 June 2006 ECA Vol.30I, P-4.072 (2006)

FLR effects in nonlinear tearing mode reconnection

N. F. Loureiro,[a,b] S. C. Cowley,[c,d] W. D. Dorland,[a]
G. W. Hammett,[b] and A. A. Schekochihin[d]

[a] *CMPD, University of Maryland, College Park, MD 20742, USA*
[b] *PPPL, Princeton University, Princeton, NJ 08543, USA*
[c] *Department of Physics and Astronomy, UCLA, Los Angeles, CA 90024, USA*
[d] *Department of Physics, Imperial College, London SW7 2BW, UK*
[e] *DAMTP/CMS, University of Cambridge, Cambridge CB3 0WA, UK*

Introduction Magnetic reconnection is a plasma physics phenomenon whereupon magnetic field lines which are being convected with the flows in the plasma suddenly break and reconnect in a different configuration. Magnetic energy is released in this process, giving rise to high velocity plasma flows, energetic particles and plasma heating. Reconnection is widely believed to be the cause of solar flares; it is also manifest in the interaction between the solar wind and the Earth's magnetic field in the magnetopause and magnetotail. In fusion devices it plays a crucial role in the development of the sawtooth instability, which has potentially disastrous consequences to the plasma confinement.

In many plasmas of interest it has long been suspected that an MHD description is too simple to fully explain the complexity of the observations. The discrepancy is obvious in the observed and calculated reconnection rates which, in the MHD framework, differ by several orders of magnitude. Interest has diverged to non-MHD effects which might cause a speed-up of this process. The potential candidates differ depending on the specific geometry and plasma parameters. For example, in most present fusion plasmas, the ion Larmor radius should exceed, or at least be comparable to, the width of the dissipation region. Thus, ion finite Larmor radius (FLR) effects cannot be neglected and are, in fact, known to produce a speed up of the reconnection rate [1]. From the numerical point of view, the FLR terms bring about one further complication: they introduce the Kinetic Alfvén wave (KAW) into the system, which has a dispersive character, i.e., $\omega \sim k_\perp^2$ (the counterpart to this in the absence of a strong magnetic field is the Hall term in Ohm's law, which also introduces a dispersive wave, the whistler). Explicit numerical integration schemes show great difficulties in coping with this wave, the time step being thus set to an impractically low value. Building on previous work [2, 3] we present a new semi-implicit method that stabilizes the KAW and the Alfvén wave (AW), while remaining accurate in the linear and nonlinear regimes. Timestep enhancements over the CFL condition of ~ 100 are obtained. Comparison with a fully explicit calculation is presented and preliminary linear and nonlinear results are briefly discussed.

Model We treat a two-fluid, two-field gyrofluid model, describing the evolution of a plasma in the presence of a strong, out-of-plane, magnetic field B_z (the guide field):

$$\frac{\partial n_e}{\partial t} + [\phi, n_e] = [\psi, \nabla_\perp^2 \psi] + \nu \nabla_\perp^2 n_e - \nu_1 \nabla_\perp^4 n_e \quad (1)$$

$$\frac{\partial \psi}{\partial t} + [\phi, \psi] = \rho_s^2 [n_e, \psi] + \eta \nabla_\perp^2 (\psi - \psi_{eq}) - \eta_1 \nabla_\perp^4 (\psi - \psi_{eq}) \quad (2)$$

$$n_e = \frac{1}{\rho_i^2} \left[\hat{\Gamma}_0(b) - 1 \right] \phi \quad (3)$$

where n_e is the perturbed electron density, ψ is the magnetic flux, related to the in-plane magnetic field by $\boldsymbol{B}_\perp = \boldsymbol{e}_z \times \boldsymbol{\nabla} \psi$, $[P, Q] = \partial_x P \partial_y Q - \partial_y P \partial_x Q$ is the Poisson bracket, ρ_i

and ρ_s are the ion and the ion-sound Larmor radius, respectively. The parallel current density is defined as $j_\parallel = \nabla_\perp^2 \psi$. Dissipation is provided by the viscosity ν and the resistivity η. We also add, for numerical convenience, phenomenological hyper-diffusion coefficients, ν_1 and η_1. These equations are reminiscent of the more complete model of Schep *et al.* [4]. Equation (3) is known in the literature as the gyrokinetic Poisson law [5]. The integral operator $\hat{\Gamma}_0$ expresses the average of the potential over rings of radius ρ_i. In Fourier space, this operator becomes $\Gamma_0(b) = e^{-b} I_0(b)$, where $b = k_\perp^2 \rho_i^2$ and I_0 is the modified Bessel function of zeroth order.

Numerical details Equations (1–3) are discretized in k-space as follows (k-space indices omitted for simplicity):

$$\begin{aligned}
\psi^{n+1,p+1} &= \frac{1}{1+\mathcal{L}+\Delta t\theta_D\left(\eta k_\perp^2+\eta_1 k_\perp^4\right)}\times \\
&\left\{\left[1-\Delta t(1-\theta_D)\left(\eta k_\perp^2+\eta_1 k_\perp^4\right)\right]\psi^n + \right. \\
&\Delta t\left[\theta G\left(n_e^{n+1,p},\phi^{n+1,p},\psi^{n+1,p}\right)+(1-\theta)G\left(n_e^n,\phi^n,\psi^n\right)\right]+ \\
&\left.\Delta t\left(\eta k_\perp^2+\eta_1 k_\perp^4\right)\psi_{eq}+\mathcal{L}\psi^{n+1,p}\right\} \qquad (4)
\end{aligned}$$

$$\begin{aligned}
n_e^{n+1,p+1} &= \frac{1}{1+\Delta t\theta_D\left(\nu k_\perp^2+\nu_1 k_\perp^4\right)}\times \\
&\left\{\left[1-\Delta t(1-\theta_D)\left(\nu k_\perp^2+\nu_1 k_\perp^4\right)\right]n_e^n + \right. \\
&\left.\Delta t\left[\theta F\left(n_e^{n+1,p},\phi^{n+1,p},\psi^{n+1,p+1}\right)+(1-\theta)F\left(n_e^n,\phi^n,\psi^n\right)\right]\right\} \qquad (5)
\end{aligned}$$

$$\phi^{n+1,p+1} = \frac{\rho_i^2}{\Gamma_0(b)-1} n_e^{n+1,p+1} \qquad (6)$$

with $n_e^{n+1,0} = n_e^n$, $\phi^{n+1,0} = \phi^n$, $\psi^{n+1,0} = \psi^n$ and $p = 0, ..., p_{max}$ with $p_{max} \geq 1$. The nonlinear terms denoted by $F(n_e, \phi, \psi)$ and $G(n_e, \phi, \psi)$ represent the Poisson brackets. In these equations $\mathcal{L}$ denotes the semi-implicit operator, defined as:

$$\mathcal{L} = k_\perp^4 \left(\rho_s^2 - \frac{\rho_i^2}{\Gamma_0 - 1}\right) a_0^2 B_{\perp,max}^2 \Delta t^2, \qquad (7)$$

where $B_{\perp,max} = \sqrt{B_{x,max}^2 + B_{y,max}^2}$ is the maximum magnitude of the in-plane magnetic field, updated at each new timestep. The parameters θ, θ_D must lie in the interval $0.5 \leq \theta, \theta_D \leq 1$. Choosing $\theta = 0.5 + \epsilon$ is useful to provide some damping of the high frequency modes. θ_D is set to 1, thus making the diffusive step only first order accurate in time. The reason for this choice stems from the fact that the timesteps that can be taken by this method are large, such that $\eta k_\perp^2 \Delta t \sim \mathcal{O}(1)$. In this limit, only the choice of $\theta_D = 1$ can recover the correct answer.

The error introduced by the semi-implicit operator $\mathcal{L}$ can be quantified by the following expression:

$$\mathcal{E}_{ji}^{p+1} = \left| \frac{\mathcal{L}\left(\psi_{ji}^{n+1,p+1} - \psi_{ji}^{n+1,p}\right)}{\sqrt{\frac{1}{N}\sum_{ji}\left|\psi_{ji}^{n+1,p+1} - \psi_{ji}^n\right|^2}} \right|, \qquad (8)$$

where $N = k_x^{max} \times k_y^{max}$. This is used to control the accuracy of the integration, and acts to increase or decrease the timestep so as to satisfy the condition $\max|\mathcal{E}_{ji}^p| < \mathcal{E}^{max}$.

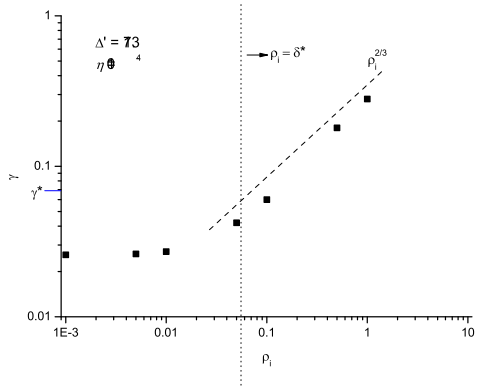

FIG. 1: Plot of the linear growth rate as a function of ρ_i at $\Delta' = 17.3, \eta = 10^{-4}, \nu = 0$. γ^* and δ^* represent, respectively, the values of the growth rate and current layer width when $\rho_i, \rho_s = 0$.

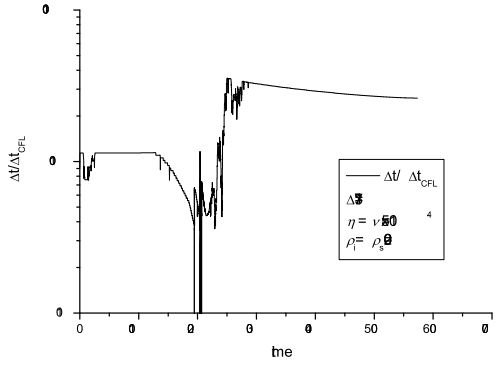

FIG. 2: Ratio of the timestep taken by the semi-implicit method to that allowed by the CFL condition (assumed CFL fraction = 0.3).

Setup The equilibrium is defined by $\psi^{(0)} = \psi_0/\cosh(x)^2$ and $\phi^{(0)} = 0$. We set $\psi_0 = 3\sqrt{3}/4$ so that the maximum value of the equilibrium magnetic field is 1. The hyper-resistivity η_1 and hyper-viscosity ν_1 are grid dependent, and their value is calculated at each time step, according to the formula $\eta_1 = \nu_1 = 0.1\ \omega_{max}/k^4_{\perp,max}$, where ω_{max} is the maximum KAW frequency based on the linear dispersion relation. Tests have been performed to certify that these coefficients are sufficiently low not to alter the physics of the system. The tearing mode instability is initialized by perturbing this equilibrium with $\psi^{(1)} = -10^{-5}\cos(2\pi/L_y\ y)$. Equations (4–6) are numerically integrated using a pseudo-spectral code.

Linear results A scan of the linear growth rate with ρ_i is shown in Figure 1. The growth rate is defined as $\gamma = d\ln\psi^{(1)}_X/dt$, where $\psi^{(1)}_X = \psi^{(1)}(x = 0, y = 0, t)$ is the reconnected flux at the X-point. As seen, γ is considerably enhanced as ρ_i becomes larger than the linear layer width in the cold plasma limit (i.e., $\rho_i = \rho_s = 0$). In this limit, the analytically predicted scaling of $\gamma \sim \rho_i^{2/3}$ is obtained.

Nonlinear results To check the accuracy of the semi-implicit scheme described above, we show in Figure 3 the contour plots of the fields obtained with a fully explicit integration (top row) and with the SI method (bottom row), setting $\mathcal{E}^{max} = 10^{-3}$ and $p_{max} = 2$. No discernible differences are observed, while the timestep enhancement over the CFL value is on the order of ~ 100, as shown in Figure 2. The overshoots at $t \approx 200$ are due to code restarts at those times, when the resolution in the y-direction was doubled. The initial resolution is 3072×128 Fourier modes. After the final doubling, which occurs at $t = 206.9$, the run resolution is 3072×1024. For further testing of the SI algorithm, we have also performed a calculation at $\rho_i = \rho_s = 0.1$. Again we obtain similar time step enhancements (not shown). Contour plots for the fields are shown in Figure 4. At these large values of ρ_i, ρ_s, the FLR terms completely dominate the dynamics, as seen from the very different structures of the fields compared to those of Figure 3. Of particular interest is the replacement of the current-sheet obtained at the lower values of ρ_i, ρ_s with a Petschek-like X-point. Further investigation of the role of ion FLR in the linear and